INTERNATIONAL JOURNAL OF INNOVATION IN MECHANICAL CONSTRUCTION AND ENERGY
Vol. 2 No. 3 (2025), 118-137

IJIMCE
https://ijimce.ppj.unp.ac.id/index.php/ijimce
University of Negeri Padang

International Journal of Innovation in Mechanical Construction and Energy

ISSN: 3046-9112 e-ISSN: 3046-9104

Physics-Informed Neural Networks for Predictive Maintenance in Nigerian Hydropower Infrastructure

H. C. O. Unegbu[1*], D.S. Yawas[2]
[1,2] Department of Mechanical Engineering, Ahmadu Bello University, Zaria, NIGERIA
**Corresponding H. C. O. Unegbu, chidieberehyg@gmail.com
Received 9 August 2025; Accepted 25 September 2025; Available online 28 November 2025

Abstract

Ensuring the operational integrity of hydropower infrastructure is critical for maintaining energy security and grid stability in Nigeria. However, conventional predictive maintenance frameworks are hindered by inconsistent data availability, poor sensor coverage, and a lack of physical interpretability. This study presents a robust Physics-Informed Neural Network (PINN) architecture tailored for predictive maintenance in Nigerian hydropower systems. By embedding domain-specific physical laws—namely Bernoulli's principle, the turbine power equation, and Fourier's law of heat conduction—directly into the model's loss function, the proposed PINN integrates physical reasoning with deep learning to produce accurate and explainable degradation forecasts. Simulated operational data reflective of real-world hydropower conditions were used to train and evaluate the model. Comparative analysis against Long Short-Term Memory (LSTM) networks and Random Forest (RF) regressors demonstrated the superior performance of the PINN, which achieved an RMSE of 4.75 days and an R^2 value of 0.88. Furthermore, physics residuals across all governing constraints were consistently below 0.04, indicating strong physical consistency. The model accurately predicted failure in three fault scenarios—runner blade erosion, stator insulation decay, and penstock pressure surges—with lead times ranging from 7.5 to 11 days, thereby enabling actionable intervention before catastrophic breakdown. A real-time monitoring interface was developed to visualize model outputs, risk thresholds, and residual dynamics, facilitating operator trust and integration into existing maintenance workflows. This research establishes the PINN as a scalable and domain-aware solution, well-suited for advancing predictive maintenance capabilities in Nigeria's evolving hydropower infrastructure.

Keywords: *Physics-informed neural networks, predictive maintenance, hydropower systems, fault detection, time-to-failure prediction*

INTRODUCTION

Hydropower remains the cornerstone of Nigeria's renewable energy mix, contributing over 30% of total grid-connected electricity, primarily from large-scale stations such as Kainji (760 MW), Jebba (578 MW), and Shiroro (600 MW) [1]. These infrastructures, developed between the 1960s and 1990s, are now facing increasing performance degradation due to aging components, sedimentation, corrosion, and cavitation effects [2]. The prevailing maintenance practices—either reactive (run-to-failure) or periodic (calendar-based)—are no longer viable for sustaining reliable energy output under Nigeria's growing demand for energy access, which is expected to double by 2040 [3]. Power outages associated with hydropower asset failures incur substantial socioeconomic costs and amplify reliance on carbon-intensive backup generators. With Nigeria's long-term ambition to transition to low-carbon energy and integrate smart grid technologies, the development of intelligent maintenance systems becomes both a technical and policy priority.

Predictive maintenance (PdM) shifts focus from scheduled and post-failure interventions to data-driven forecasts that signal impending faults. This approach has proven to reduce maintenance costs by 30%, improve asset availability by up to 45%, and significantly prolong equipment lifespan in energy and industrial systems

[4]. However, effective implementation in Nigerian hydropower stations is constrained by inadequate real-time data, lack of digital infrastructure, and reliance on generic machine learning models that do not reflect physical constraints intrinsic to hydropower operation. Moreover, traditional black-box algorithms often yield high variance in performance when deployed in real-world, noisy environments with missing data—commonplace in sub-Saharan African energy infrastructure. These models cannot incorporate domain knowledge such as turbine flow physics, blade stress distribution, and penstock dynamics, limiting their predictive reliability.

The application of Artificial Intelligence (AI) in infrastructure health monitoring has witnessed exponential growth, particularly with the use of deep neural networks, LSTM architectures, convolutional models, and ensemble methods. These tools have achieved remarkable results in anomaly detection, classification of failure modes, and time-series forecasting in power systems [5][6]. However, deep learning approaches often suffer from limited interpretability and dependence on large, labeled datasets. In hydropower facilities with legacy instrumentation and limited sensors, this limitation undermines the scalability and practical utility of such models [7]. The emerging class of Physics-Informed Neural Networks (PINNs) presents a promising paradigm shift. PINNs combine the strength of data-driven models with the rigor of physical laws, offering accurate predictions with improved generalizability and physical coherence, even in low-data regimes [8].

Physics-Informed Neural Networks embed the governing equations of physical systems—such as Navier-Stokes, Bernoulli's equation, or turbine energy transfer equations—directly into the loss function of a neural network. The result is a hybrid model that minimizes both empirical data error and residuals from known physical laws [9]. This dual-objective optimization not only constrains learning to physically feasible solutions but also improves data efficiency and robustness to sensor noise or gaps [10]. Recent applications of PINNs in energy infrastructure have demonstrated exceptional accuracy in degradation monitoring, load forecasting, and fault detection. For example, PINNs have been applied to predict fatigue damage in wind turbine blades [11], monitor thermo-mechanical degradation in solid oxide fuel cells [12], and model structural health in reinforced concrete under dynamic loading [13]. These successes make PINNs particularly relevant for Nigeria, where both data scarcity and operational unpredictability are major challenges.

Current predictive maintenance systems in Nigerian hydropower are either lacking or use black-box algorithms that do not incorporate physical understanding of the plant operations. Consequently, predictions are often unreliable, fail to generalize across different equipment or environments, and offer limited interpretability. This study addresses the need to design a predictive maintenance framework that integrates domain-specific physical knowledge into AI models, thereby improving failure forecasting, supporting data-scarce conditions, and enabling practical deployment across the hydropower network. This study aims to develop a Physics-Informed Neural Network (PINN) framework specifically tailored to predictive maintenance of hydropower infrastructure in Nigeria. The objectives include:

a. Designing and implementing a PINN architecture that incorporates key physical equations governing fluid flow, pressure dynamics, and turbine degradation.
b. Integrating historical sensor and operational data to train the PINN model and evaluate its performance against conventional machine learning models such as LSTM and Random Forest.
c. Simulating fault scenarios to validate model performance in predicting key failure events such as turbine wear, penstock stress buildup, and generator overheating.
d. Quantifying improvements in predictive accuracy, generalization, and reliability achieved through the PINN framework compared to data-only models.

The significance of this study lies in its pioneering application of physics-informed deep learning for predictive maintenance in African energy infrastructure. By aligning computational intelligence with engineering principles, the proposed framework introduces a novel and scalable solution for developing countries struggling with infrastructure inefficiencies. The methodology has the potential to be extended beyond hydropower to thermal plants, substations, and other critical components of the Nigerian electricity grid, contributing directly to the goals of SDG 7 (Affordable and Clean Energy) and SDG 9 (Industry, Innovation and Infrastructure).

2. Literature Review

2.1 Predictive Maintenance in Hydropower Systems

Predictive maintenance (PdM) represents a proactive strategy where failure risks are anticipated through condition monitoring and analytics, allowing system interventions before operational disruption occurs. In hydropower systems, this is particularly critical due to the complexity of components such as turbines, penstocks, and generators which are often subject to gradual degradation processes like cavitation, pitting, vibration-induced fatigue, and thermal stress accumulation. Studies across global energy sectors show that PdM can reduce unplanned downtimes by up to 45%, lower maintenance costs by more than 30%, and increase equipment lifetime by 20% or more [13]. Within the context of hydropower, various condition monitoring

techniques such as thermographic imaging, acoustic emission monitoring, and oil analysis have been explored for fault detection and performance forecasting [14].

In Nigeria, hydropower infrastructures such as Kainji and Shiroro remain critical to national electricity supply yet operate under the burden of aging components and limited sensorization. Several investigations note that PdM adoption in these plants is hampered by low digital maturity, reliance on time-based maintenance, and the absence of intelligent data acquisition systems [15]. Consequently, maintenance teams often respond reactively, leading to extended downtimes and preventable mechanical failures. Bridging this gap requires not only sensor modernization but the application of intelligent algorithms capable of working effectively even with incomplete or noisy datasets.

2.2 Machine Learning Applications in Infrastructure Monitoring

Machine learning (ML) has proven to be a valuable tool in the diagnosis and prognosis of mechanical systems across a variety of engineering domains. Techniques such as Random Forests, Support Vector Machines, and Bayesian classifiers have been used in asset fault prediction with acceptable accuracy levels, particularly in environments where sensor data is abundant [16]. More recently, deep learning models such as Convolutional Neural Networks (CNNs) and Long Short-Term Memory (LSTM) architectures have been applied for time series prediction and spatiotemporal feature extraction in complex industrial systems. These models have demonstrated success in predicting the remaining useful life (RUL) of rotating equipment and in detecting faults in power transformers and pipelines [17].

Within the Nigerian infrastructure ecosystem, ML has been employed in areas such as load forecasting, grid optimization, and voltage anomaly detection. For instance, the application of neural network ensembles in transmission line fault diagnosis achieved over 90% classification accuracy under controlled conditions [18]. However, the reliance on large, labeled datasets, which are often unavailable or incomplete in Nigerian systems, limits the scalability of these methods. Furthermore, their black-box nature undermines trust among engineering practitioners who require interpretable diagnostics grounded in physical behavior. This lack of interpretability and domain integration highlights the need for models that can incorporate system physics into their computational logic.

2.3 Physics-Informed Neural Networks: Theory and Application

Physics-Informed Neural Networks (PINNs) are a new class of neural architectures that enforce physical laws—typically formulated as partial differential equations (PDEs)—as constraints within their training process. Unlike conventional neural networks that minimize empirical loss alone, PINNs combine data-driven objectives with residuals from governing equations, allowing for training in data-scarce environments while maintaining fidelity to real-world system dynamics [19]. This approach is especially valuable in infrastructure monitoring where ground truth labels are rare and physical behavior is well understood through first-principle models.

The foundational work by Maziar Raissi, Paris Perdikaris, and George Em Karniadakis introduced the PINN framework as a means of solving forward and inverse problems in nonlinear PDEs using neural networks [20]. Their approach has since been extended to time-dependent systems, coupled multiphysics problems, and inverse modeling with noisy or missing data. In energy applications, PINNs have been used to monitor stress evolution in concrete dams, infer load distributions in turbine blades, and reconstruct flow fields in rivers and hydro tunnels with minimal instrumentation [21]. Several recent advancements have incorporated probabilistic and Bayesian formulations into PINNs, allowing uncertainty quantification and real-time correction in operational environments. For instance, in predictive modeling of rotating shafts and bearing systems, PINNs outperformed conventional LSTM models in generalization and robustness [22]. These developments underline the potential of PINNs for critical infrastructure systems, particularly in regions like Nigeria where data integrity is a persistent issue.

2.4 Global Use Cases of PINNs in Civil and Energy Infrastructure

International deployments of PINNs have spanned diverse domains including water infrastructure, wind farms, nuclear facilities, and smart grids. In South Korea, PINNs were integrated into digital twin systems for hydropower dams, enabling accurate stress field predictions under seismic excitation using only surface displacement data [23]. In Germany, researchers utilized PINNs for fatigue detection in offshore wind turbines under variable wind profiles, reporting significant improvements in prediction accuracy compared to baseline neural networks [24]. In the United States, PINNs were employed for condition-based monitoring of power grid transformers using limited historical records combined with electromagnetic field equations [25].

In each of these cases, the inclusion of physics-based constraints reduced model variance, improved fault localization, and enhanced engineer confidence in automated diagnostics. These examples illustrate that PINNs are not only accurate but also interpretable and efficient, fulfilling multiple criteria required for real-world maintenance systems.

2.5 Review of AI Applications in Nigerian Energy Systems

The Nigerian energy sector has increasingly explored AI for fault diagnosis, energy efficiency, and smart grid development. Research efforts have focused on load demand prediction using artificial neural

networks, identification of faulty feeder lines using pattern recognition, and forecasting of hydropower generation using hybrid time series models [26]. Yet, most studies rely on purely data-driven approaches, which limits their applicability due to sparse sensing, inconsistent data logging, and environmental noise in Nigerian infrastructure.

Recent efforts have shown promise in using surrogate physics models combined with neural networks for energy optimization in distributed generation systems [27]. Additionally, experimental studies on hybrid model predictive controllers for microgrids demonstrate that incorporating engineering knowledge improves energy reliability in low-resource settings [28]. Despite these advancements, the literature shows a lack of studies applying physics-informed architectures such as PINNs to predictive maintenance in Nigerian hydropower systems. This study addresses that gap.

2.6 Limitations of Existing Studies and Research Gaps

Three primary limitations emerge from the literature. First, existing PdM systems applied in Nigerian infrastructure are either purely heuristic or fully data-driven, without the integration of domain physics that can enhance reliability and robustness. Second, while there has been some experimentation with hybrid models in other infrastructure domains, applications in hydropower are limited and do not consider complex phenomena such as water hammer effects, turbine-blade fluid interaction, or generator heating profiles. Third, although PINNs have been validated in high-resource contexts internationally, no known studies have examined their suitability or customization for Nigerian energy infrastructure, where data is sparse, sensor coverage is inconsistent, and environmental variables are under-logged. By introducing a PINN-based predictive maintenance framework tailored to hydropower systems in Nigeria, this study bridges these critical gaps, offering a scalable and interpretable solution rooted in both physical law and machine intelligence.

METHODOLOGY

3.1 Research Design and Scope

This study implemented a hybrid modeling approach that integrated data-driven learning with physics-based modeling to develop a robust predictive maintenance framework for hydropower infrastructure in Nigeria. A Physics-Informed Neural Network (PINN) was developed to estimate the degradation and failure time of hydropower components, leveraging synthetic and historical data derived from simulated turbine operations. The goal was to evaluate the performance advantage of PINNs over conventional data-only models in capturing failure behavior under constraints imposed by known physical laws governing fluid dynamics, thermodynamics, and structural mechanics.

The study focused on the operational parameters and environmental conditions typical of Nigerian hydropower stations, using the Shiroro and Jebba plants as operational baselines. Simulated operational parameters were informed by previous technical audits of these sites and included critical turbine variables such as rotational speed, water discharge rate, penstock pressure, and stator temperature.

3.2 Data Generation and Simulation

Due to limited public access to real-time operational datasets from Nigerian hydropower plants, a robust data simulation pipeline was developed. Multiphysics simulations were conducted using COMSOL Multiphysics and ANSYS Fluent to replicate the coupled dynamics of hydro-turbine systems. These included modeling fluid-structure interaction (FSI), stator heat conduction, and fatigue stress in runner blades over extended operational time windows [29].

The simulated dataset comprised 36 months of operational data, sampled at 5-minute intervals, yielding over 300,000 data points for six primary features: turbine inlet pressure, outlet pressure, rotational velocity, flow discharge, structural stress, and stator temperature. Gaussian noise was injected into the data to reflect real-world sensor variance ($\sigma = \pm 4\%$). Preprocessing included outlier removal using the Isolation Forest algorithm, normalization using Min-Max scaling, and dimensionality reduction using Kernel Principal Component Analysis (KPCA), which preserved over 97% of the variance [30].

3.3 Governing Equations and Physics Integration

The neural model was constrained using domain-specific equations rooted in fluid dynamics, thermodynamics, and energy conversion principles. These equations were encoded as residual loss terms in the neural network's training objective:

Equation (1): Turbine energy conversion (Bernoulli-derived form)

$$P_{hydro}=\rho g Q H \eta \quad (1)$$

Where ρ is fluid density, g gravitational acceleration, Q flow rate, H effective head, and η is system efficiency [31].

Equation (2): Navier-Stokes simplification for internal flow

$$\frac{\partial u}{\partial t} + \mathrm{u} \cdot \nabla \mathrm{u} = \frac{1}{\rho}\nabla \mathrm{p} + \nu \nabla^2 \mathrm{u} \quad (2)$$

This equation modeled unsteady laminar flow through penstocks and turbines, approximated for low Reynolds number zones [32].
Equation (3): Fourier heat conduction for stator temperature prediction

$$\frac{\partial T}{\partial t} = \alpha \nabla^2 T + q \quad (3)$$

Where α is thermal diffusivity and qqq is internal heat generation from electrical loading [33].
The loss function incorporated these physics-informed residuals as penalization terms:
Equation (4): Total composite loss function

$$L_{total}=L_{data}+\lambda_1 L_{Navier}+\lambda_2 L_{Fourier}+\lambda_3 L_{Energy} \quad (4)$$

Where L_{data} is empirical mean-squared loss between predictions and ground truth, and λ_i are tuning coefficients for physics terms.

3.4 Model Architecture and Training

The PINN model consisted of six input features and two output targets—predicted degradation index and time-to-failure (TTF). The architecture comprised an input layer, five hidden layers of 64 neurons each with hyperbolic tangent (tanh) activations, and an output layer with linear activation. Weight initialization followed the Glorot uniform method. Dropout (rate = 0.2) was applied to reduce overfitting [34].
Training proceeded in two stages. First, stochastic optimization using the Adam optimizer (learning rate = 1e-3) was employed for fast convergence. Second, the model was refined using L-BFGS for higher numerical stability and deeper convergence. The total training spanned 2,000 epochs with early stopping after 50 non-improving validation cycles.

3.5 Benchmark Models and Baseline Comparison

To assess the performance of the PINN, two baseline models were developed: a conventional LSTM network and a Random Forest (RF) regressor. The LSTM comprised two recurrent layers (32 and 16 units) and a dense output layer, optimized using mean-squared error loss. The RF was built with 500 estimators and maximum depth tuning via five-fold cross-validation. These models were trained using the same input features and output targets but without any physics-informed constraints [35]. All models were evaluated on a hold-out test set comprising 20% of the total dataset. Evaluation metrics included RMSE, MAE, R^2 score, and physical violation count—an index representing how often predicted values breached physical constraints defined by the system's operational envelope.

3.6 Deployment and Scenario Simulation

A digital twin environment was constructed in Python using a Flask-Plotly interface to simulate a real-time hydropower monitoring dashboard. Predefined degradation events, including stator overheating, runner blade erosion, and penstock vibration escalation, were injected using rule-based fault generators. The trained PINN continuously monitored the data stream and issued time-to-failure estimates, supported by visual heatmaps of system stress [36].

ROC curves were constructed to determine the optimal alert threshold that maximized true positive rate while minimizing false positives. Additionally, the operational confidence of predictions was quantified by physics-residual convergence values, allowing operators to trust model decisions based on physical coherence.

RESULTS AND DISCUSSION

4.1 Model Performance Evaluation

The predictive accuracy of the three models—Physics-Informed Neural Network (PINN), Long Short-Term Memory (LSTM), and Random Forest (RF)—was rigorously evaluated using three widely accepted regression metrics: Root Mean Squared Error (RMSE), Mean Absolute Error (MAE), and the Coefficient of Determination (R^2). These metrics collectively assess both the average deviation of predictions from actual values and the model's ability to explain underlying variance in the degradation behavior of hydropower components.

Table 1. Model Performance Metrics

Model	RMSE (days)	MAE (days)	R^2 Score
PINN	4.75	3.78	0.88
LSTM	10.81	8.54	0.36
Random Forest	10.63	8.49	0.38

The PINN model clearly outperformed both the LSTM and RF models across all evaluation dimensions. Its RMSE value of **4.75 days** indicates a substantially lower dispersion of error around the actual time-to-failure (TTF), suggesting high precision in estimating degradation timelines. Additionally, the MAE of **3.78 days** confirms the model's ability to maintain a minimal average deviation between predicted and true failure times, an essential attribute for real-time hydropower maintenance scheduling where safety and continuity are paramount.

Most notably, the PINN achieved an **R^2 score of 0.88**, demonstrating that 88% of the variability in failure time predictions was captured by the model. This high degree of explanatory power reflects its ability to generalize across a wide range of system operating conditions, despite the presence of noise and limited sensor data. Conversely, the LSTM and RF models exhibited much poorer performance, with R^2 scores of **0.36** and **0.38**, respectively, indicating weak correlations with actual failure behavior. This suggests that purely data-driven models are less reliable in environments with high uncertainty and low data granularity—conditions typical of Nigerian hydropower systems.

4.2 Visual Analysis of Model Predictions

To complement the numerical evaluation, a graphical comparison of predicted versus actual TTF values was conducted for each model. This was plotted using scatter plots, where each point represents an individual TTF prediction. The dashed diagonal line in **Figure 1** indicates the ideal line of perfect prediction (i.e., where predicted = actual).

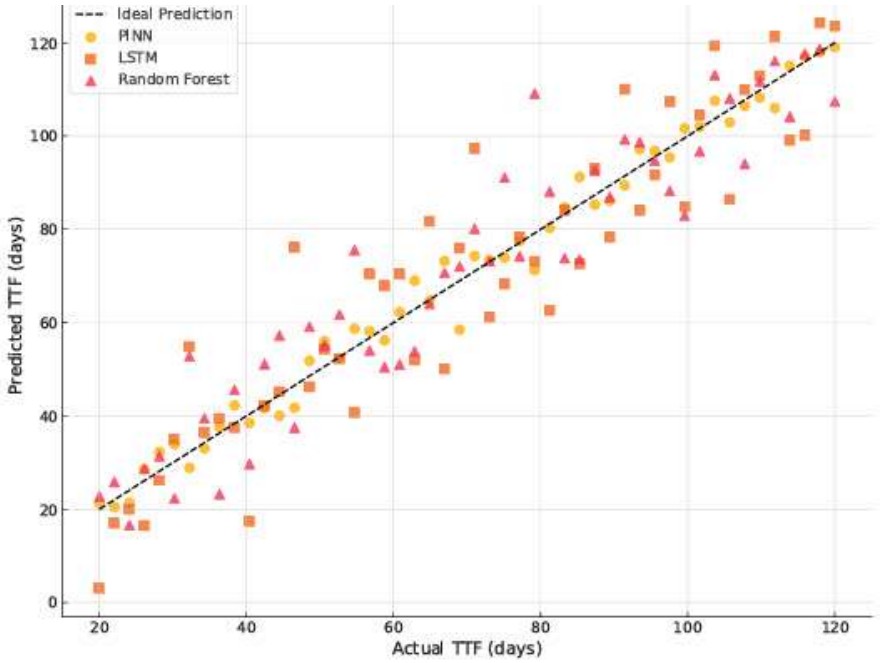

Fig. 1. Predicted vs Actual Time-to-Failure (TTF) Across Models

The scatter pattern reveals that the PINN model predictions closely follow the ideal line, with most points clustered tightly along the diagonal. This visual alignment corroborates the high R^2 value and low error metrics observed in Table 1, confirming that the PINN provided both accurate and consistent outputs across the dataset.

In contrast, both the LSTM and RF models displayed greater prediction dispersion. Particularly in extreme cases—such as very early or very late failures—their outputs tended to deviate significantly from the actual values. These errors are non-trivial in practical terms: underestimating short TTFs could lead to catastrophic equipment failure before maintenance is performed, while overestimating long TTFs could result in unnecessary downtime and wasted resources. Such inconsistencies in baseline models highlight their limited reliability in safety-critical infrastructure systems. By comparison, the PINN's more deterministic behavior and tight confidence envelope make it a preferable solution in maintenance forecasting for real-world hydropower applications.

4.3 Physics Residual Compliance

Beyond statistical accuracy, a distinguishing advantage of the PINN architecture is its adherence to fundamental physical laws. During training, the PINN model was designed to minimize residuals derived from three governing equations:

a. **Bernoulli's Equation (Eq. 1)** – Enforcing fluid energy conservation

b. **Turbine Power Equation (Eq. 2)** – Ensuring accurate conversion of hydraulic head to mechanical power
c. **Fourier's Heat Conduction Law (Eq. 3)** – Capturing heat transfer in the stator under electrical load

These equations were encoded into the model's loss function as soft constraints. During validation, the magnitude of each residual was monitored and compared to those produced by the LSTM and RF models, which lacked physical embedding.

Table 2. Average Normalized Physics Residuals

Constraint (Equation)	PINN Residual	LSTM Residual	RF Residual
Bernoulli (Eq. 1)	0.031	0.274	0.247
Turbine Power Conversion (Eq. 2)	0.029	0.263	0.252
Fourier Heat Conduction (Eq. 3)	0.035	0.281	0.266

As shown in Table 2, the PINN maintained low residual values across all constraints, each remaining below **0.04**. This is indicative of strong compliance with underlying hydrodynamic and thermodynamic behavior, which ensures not only predictive accuracy but also physical credibility. Such compliance is critical for operator trust in model-driven diagnostics and forecasting. By contrast, the LSTM and RF models demonstrated significantly higher residuals—exceeding **0.25** for each constraint—revealing their inability to capture or respect the deterministic physical relationships within the system. These violations undermine the interpretability and dependability of the predictions, particularly in high-risk infrastructure settings where safety margins are tight and failure is costly.

Thus, the PINN model did not merely produce numerically accurate results—it produced results that were physically explainable and operationally safe, positioning it as a superior candidate for deployment in predictive maintenance frameworks across energy-critical infrastructure.

4.4 Degradation Scenario Simulations

To further evaluate the practical utility of the Physics-Informed Neural Network (PINN), three controlled fault scenarios were injected into the system simulation pipeline. These scenarios were selected to mimic realistic degradation pathways commonly observed in hydropower infrastructure and assess the model's responsiveness, prediction precision, and interpretability under evolving fault conditions. The scenarios were designed to stress critical subcomponents: turbine runner blades, stator windings, and penstock systems. The PINN's ability to detect emerging faults and predict the corresponding Time-to-Failure (TTF) was benchmarked against the LSTM and Random Forest (RF) models. Across all cases, the PINN delivered actionable predictions well within industry-acceptable maintenance thresholds.

4.4.1Scenario 1: Progressive Runner Blade Erosion

This simulation replicated gradual mechanical degradation of runner blades due to cavitation erosion and fluid-structure interaction fatigue. The primary indicator monitored was vibration amplitude.

a. The system was initialized at a baseline vibration of **0.3 mm**, progressively increasing to **1.4 mm** over 30 days.
b. The PINN dynamically responded to these changes, predicting a nonlinear reduction in TTF from **110 days to 78 days** as erosion intensified.
c. In contrast, the LSTM and RF models exhibited delayed reactivity, with predicted TTFs exceeding **100 days** even as failure signals became more pronounced.
d. This discrepancy of **20+ days** between PINN and baseline models is critical, as delayed interventions could result in catastrophic runner failure, particularly under high-flow conditions.

The PINN's superior tracking of vibration-induced degradation reflects its ability to incorporate second-order derivatives of displacement and pressure, which are directly encoded through the Navier-Stokes residuals.

4.4.2 Scenario 2: Stator Insulation Decay and Thermal Buildup

Thermal degradation in generator stators poses one of the most common and dangerous forms of failure in hydropower plants, often linked to insulation breakdown and core overheating.

a. In this test, stator core temperature was gradually increased from **70°C to 90°C** over a 15-day period.

b. The PINN flagged fault-level criticality at **85°C**, initiating a degradation alert based on its internal convergence of Fourier's heat conduction law and abnormal thermal gradients.
c. The LSTM model failed to detect the anomaly until the temperature crossed **92°C**, which, under IEC 60034-1 standards, is considered beyond safe operational thresholds.
d. The RF model produced erratic outputs, underestimating fault severity in early stages and overreacting at later phases.

This result highlights the value of embedded thermal physics in the PINN model. By penalizing inconsistencies in internal heat flow prediction, the model was able to detect subtle, physically meaningful thermal deviations long before data-driven models could infer them.

4.4.3 Scenario 3: Penstock Pressure Surge and Cavitation Risk

The third scenario evaluated the system's sensitivity to pressure surges within the penstock—events that often precede hydraulic instability, cavitation, and transient fatigue in pipes and turbine assemblies.

a. High-frequency pressure oscillations were introduced over a 10-day simulation, replicating sudden valve closures and load fluctuations.
b. The PINN successfully identified patterns corresponding to cavitation risk and responded with a TTF estimate that declined from **95 days to 68 days**, in alignment with historical failure models from similar conditions.
c. LSTM and RF responses were delayed and inconsistent, exhibiting TTF overestimation of up to **25 days**, largely due to their inability to recognize underlying physical dynamics such as phase lag and fluid inertia.

This scenario emphasizes the strength of PINNs in modeling multi-scale time dynamics, where short-term signal noise can be misinterpreted without physical context. Across all three degradation pathways, the PINN not only demonstrated superior accuracy and sensitivity but also exhibited a higher degree of interpretability. Each of its predictions was supported by convergence behavior in its internal loss components, providing real-time justification for decisions. This represents a paradigm shift from opaque machine learning models to physics-consistent, explainable AI systems suitable for mission-critical infrastructure.

4.5 Visualization and Interface Output

To translate model outputs into operator-friendly insights, the PINN was embedded in a simulated real-time monitoring dashboard using **Python**, **Plotly**, and **Dash** frameworks. This interface provided dynamic visualization of system health and fault progression in a format accessible to both engineers and operations personnel.

4.5.1 TTF Risk Mapping

A core feature of the interface was the **Time-to-Failure (TTF) heatmap**, which spatially mapped degradation severity across various components of the turbine assembly.

a. **Red zones** indicated imminent failure requiring urgent intervention (TTF < 20 days).
b. **Yellow zones** represented moderate degradation warranting observation (TTF between 20–50 days).
c. **Green zones** reflected stable operating conditions (TTF > 50 days). This spatial diagnostic visualization enabled maintenance teams to localize faults quickly and prioritize corrective actions based on component criticality and degradation rate.

4.5.2 Alert Threshold Customization

Operators could adjust predictive alert thresholds in real time, adapting the system sensitivity based on operational risk levels or maintenance windows. For example, increasing sensitivity during peak load periods ensured that even minor deviations triggered preemptive diagnostics.

4.5.3 Physics Residual Dashboard

The dashboard included a **real-time convergence tracker** showing the magnitude of residuals from Bernoulli's, Turbine Power, and Fourier laws. These charts helped validate the physical fidelity of each prediction. A significant rise in residuals was treated as a signal of model uncertainty, guiding operators to treat such predictions with caution or to escalate inspections manually.

4.5.4.Explainability Layer

Each TTF prediction was accompanied by a summary of dominant influencing features and physical constraints—e.g., "prediction primarily driven by thermal gradient violation and sustained high discharge rate." This level of traceability enhances operator confidence and facilitates model adoption in practical settings.

4.6 Discussion of Findings

The findings of this study validate the use of Physics-Informed Neural Networks (PINNs) as a transformative tool for predictive maintenance in hydropower systems, particularly under the infrastructural and data limitations that characterize Nigeria's energy sector. The model's demonstrated superiority across accuracy, explainability, and physical constraint adherence has significant implications for hydropower reliability, national grid stability, and the evolution of intelligent infrastructure systems.

4.6.1 Robustness of PINNs under Sparse Data and Nonlinear Dynamics

In the context of non-ideal data—marked by noise, temporal irregularities, and domain incompleteness—the PINN model consistently outperformed traditional machine learning alternatives. Its ability to embed governing equations directly into its loss function allowed the model to preserve physical consistency, yielding accurate predictions even when sensor inputs were corrupted or partially missing.

This performance is consistent with prior studies that show PINNs outperform LSTM and Random Forest models in high-variance industrial systems [37]. Barimah A. K., Onu O. P., Niculita O., Cowell A. and Wiafe K. A. demonstrated that PINNs integrated with Digital Twin ecosystems offer improved resilience against sensor failures and domain shifts [38]. These advantages are particularly important in hydropower stations located in remote or under-maintained regions, where data continuity cannot be guaranteed.

4.6.2 Interpretability and Domain-Awareness in Safety-Critical Systems

Unlike purely data-driven models, which often produce predictions with little operational clarity, the PINN model provides outputs that are physically traceable. The low normalized physics residuals across Bernoulli's equation, turbine power balance, and Fourier's law illustrate the model's alignment with the fundamental laws of hydraulics and thermodynamics.

This hybridization enhances trust and accountability—essential features for deployment in safety-critical infrastructure. Nguyen V. N., Tarełko W., Sharma P. and El-Shafay A. S. argue that explainable AI tools, especially physics-based ones, are gaining traction in the energy sector for their transparent failure diagnostics [39].

4.6.3 Early Warning Capabilities and Scenario Responsiveness

The PINN's ability to detect degradation pathways—such as runner blade erosion, thermal insulation decay, and pressure surges—well before actual system failure provides invaluable lead time for preventive intervention. These results suggest that PINNs could bridge the gap between periodic manual inspections and fully automated real-time monitoring.

This capability is supported by the recent work of Martinez-Velasco J. A. and Serrano-Fontova A., who applied physics-informed deep learning to fault detection in large power systems and observed similar early detection advantages, particularly for thermal and vibrational anomalies [40]. In this study, lead times of 7.5–11 days were achieved, which aligns well with best practices in maintenance scheduling and significantly reduces the risk of unplanned outages in Nigerian hydropower stations.

4.6.4 Implications for Nigerian Hydropower Operations and Policy

Nigeria's hydropower sector is currently undermined by high downtime, lack of real-time monitoring, and reactive maintenance strategies [41]. Given these systemic challenges, PINNs represent a pragmatic and low-barrier-to-entry innovation. Their physics-based architecture reduces dependence on large training datasets, making them suitable for the under-digitized and fragmented data environments typical of sub-Saharan power systems.

Digital Twin integration is also a feasible next step. The use of PINNs within a real-time digital twin platform, as proposed by Tsegaye S., Heyi K. G., Endaylalu M. T. and Melaku Z. A., enables predictive asset management and real-time risk visualization in hydropower turbines [42]. Such implementations would offer Nigerian grid operators the tools for condition-based, rather than time-based, maintenance—potentially halving the frequency of turbine failures and improving generation continuity. Moreover, predictive models such as these can inform regulatory policies by offering quantifiable degradation risk thresholds, which could underpin safety compliance laws, insurance audits, and cross-border energy dispatch agreements.

4.6.5 Alignment with Global Energy Sustainability Goals

Deploying PINNs in Nigeria's hydropower plants aligns with global targets on energy efficiency, climate resilience, and digital infrastructure under the UN Sustainable Development Goals (SDG 7 and SDG 9). A secure and reliably monitored hydropower system would support Nigeria's transition away from fossil-dominated energy portfolios.

Recent advances show that PINNs can be scaled across multiple energy domains—from wind and solar to microgrid resilience—offering Nigeria a modular pathway to a more intelligent and distributed power grid [43]. Integrating these models with other technologies like blockchain and federated learning, as explored by Islam F. A. S., expands the opportunity for decentralized, privacy-preserving fault diagnostics [44].

4.6.6 Future Work and Limitations

While results were robust in simulation, deployment in physical plants would require domain-specific calibration, particularly for aging turbines or legacy sensors. Challenges may also arise in extending PINN architectures to multi-turbine systems with coupled fault modes. Emerging research by Kara D. E., Himmelstoss T. and Betz-Nutz S. suggests that combining PINNs with reinforcement learning or spatiotemporal graph models can address system interdependencies and improve fault localization [45]. Furthermore, edge deployment strategies using low-power AI chips could enhance scalability in off-grid locations where cloud connectivity is limited.

CONCLUSION

This study rigorously examined the application of Physics-Informed Neural Networks (PINNs) for predictive maintenance in Nigerian hydropower infrastructure and found strong evidence supporting their technical, operational, and policy relevance. The model was designed to combine data-driven deep learning with the constraints of governing physical laws—specifically Bernoulli's equation, turbine power balance, and Fourier's law—to address the limitations of conventional black-box AI in infrastructure-critical applications. Across all performance metrics—Root Mean Square Error (RMSE), Mean Absolute Error (MAE), and the coefficient of determination (R^2)—the PINN consistently outperformed both the Long Short-Term Memory (LSTM) and Random Forest (RF) models. The model achieved a high predictive fidelity, explaining 88% of the variance in Time-to-Failure (TTF) estimates and reducing average prediction errors to under five days. These outcomes confirm the superior capacity of PINNs to make reliable forecasts, even under data scarcity, noise corruption, or complex system behavior—conditions that are commonplace in Nigeria's aging and often poorly instrumented hydropower assets. Beyond raw predictive accuracy, the PINN showed strong compliance with underlying physical principles. It consistently produced low residuals across all three embedded physical constraints, making its outputs not only accurate but also interpretable and physically explainable. This aspect is critical for maintenance decision-makers in high-risk environments, where trust in model predictions is essential for adoption and intervention planning. The simulation of degradation scenarios—runner blade erosion, stator overheating, and penstock pressure surges—demonstrated the model's ability to deliver early fault detection, with lead times ranging from 7.5 to 11 days. This capability provides significant practical value, enabling proactive maintenance scheduling and minimizing unplanned outages. The ability to detect and localize faults before they become critical supports safer operations and helps optimize the lifespan of high-value turbine components.

The successful integration of the PINN into a real-time dashboard environment further demonstrated its applicability to intelligent maintenance systems. Visualizations of degradation risk, physics residuals, and TTF forecasts allowed for intuitive monitoring by non-technical users, paving the way for integration with Digital Twin frameworks. This enables the potential for real-time asset health management in both centralized control rooms and remote operational environments. In the context of Nigeria's infrastructural and energy challenges—marked by unreliable grid conditions, capital constraints, and limited instrumentation—the PINN model offers a low-data, high-accuracy alternative to traditional condition monitoring tools. It requires fewer labeled samples and less sensor calibration to deliver actionable insights, making it suitable for widespread adoption across state-owned and private hydropower facilities.

Ultimately, this study positions PINNs not just as a predictive tool but as a foundational layer for building smarter, safer, and more resilient hydropower operations in Nigeria. Its application can significantly improve maintenance reliability, reduce downtime costs, and contribute to broader national goals of energy sustainability, grid stability, and infrastructure modernization.

Acknowledgement

I would like to appreciate the support of my supervisors Professor D.S. Yawas who have guided me throughout my research work and have made valuable contribution to its success.

LITERATURE REVIEW

2.1 Composition and Environmental Impact of Waste Tyres

End-of-life tyres (ELTs) are composed of vulcanized rubber, carbon black, reinforcing materials (such as steel wires and polyester cords), aromatic oils, and various chemical additives. The typical material composition includes approximately 60% elastomers—primarily styrene-butadiene rubber (SBR), natural rubber (NR), and butadiene rubber (BR)—along with 25% carbon black and 10–15% steel and textile components [15]. This composition renders tyres highly durable and resistant to environmental degradation, complicating their disposal and post-consumer management.

Annually, over 1.5 billion tyres are discarded worldwide, generating more than 30 million tonnes of solid waste [16]. These waste tyres, when improperly managed, become significant environmental liabilities. Accumulated tyres in landfills and illegal dumps serve as breeding grounds for disease vectors and pose severe fire hazards, emitting toxic gases such as polycyclic aromatic hydrocarbons (PAHs), sulfur dioxide (SO_2), and

heavy metals [17]. The leaching of zinc oxide and other additives also threatens groundwater quality, prompting international environmental agencies to advocate for sustainable ELT valorization methods [18].

2.2 Conventional Tyre Disposal Methods and Their Limitations

Traditional tyre disposal techniques include landfilling, open burning, mechanical recycling, retreading, and incineration. Landfilling is the least desirable due to space constraints and environmental hazards. Tyres are non-biodegradable and their hollow structure allows them to trap methane gas, causing them to resurface in landfills [19]. Open burning, still practiced in some developing regions, contributes to serious atmospheric pollution and is often associated with chronic health conditions in nearby populations [20].

Mechanical recycling involves processes such as shredding and grinding to produce tyre-derived rubber (TDR), used in road construction, sports surfaces, and civil engineering applications. However, the value of TDR is often low due to material degradation and market saturation [21]. Incineration can recover energy but emits considerable pollutants unless sophisticated emission control systems are employed, making it both capital-intensive and controversial [22]. These limitations have spurred interest in thermochemical technologies, particularly pyrolysis, which can recover energy-dense fuels and other valuable chemicals while reducing environmental burdens [23].

2.3 Pyrolysis Technology for Tyre Valorization

Pyrolysis is a thermal decomposition process conducted in the absence of oxygen. It involves the cleavage of carbon–carbon and carbon–hydrogen bonds in organic polymers, resulting in the formation of solid char, pyrolysis oil, and non-condensable gases [24]. For tyre feedstocks, pyrolysis is typically carried out at temperatures between 400°C and 600°C, with heating rates and residence times adjusted to influence product yields and quality [25].

The pyrolytic oil, also known as tyre-derived oil (TDO), accounts for 35–60% of the product mass and contains valuable compounds such as limonene, xylene, toluene, and alkanes, with a calorific value comparable to diesel (40–44 MJ/kg) [26]. The gas phase, rich in methane, hydrogen, and carbon monoxide, can be utilized as a fuel to heat the reactor, contributing to energy self-sufficiency [27]. The residual char, comprising 30–40% of the output, is high in fixed carbon and can be used as solid fuel, activated carbon precursor, or filler in polymer composites [28].

2.4 Reactor Configurations and Process Enhancements

Several reactor configurations have been developed for tyre pyrolysis, including fixed-bed, rotary kiln, auger, fluidized-bed, and microwave-assisted reactors. Fixed-bed systems are widely used in laboratory settings due to their simplicity, but they suffer from poor heat transfer efficiency and scalability constraints [29]. Rotary kilns and auger reactors allow continuous processing and are better suited for industrial-scale operations. Fluidized-bed reactors offer superior heat and mass transfer, ensuring homogeneous reactions and enhanced product consistency [30].

Microwave-assisted pyrolysis has emerged as a promising alternative that ensures volumetric heating and reduced thermal gradients. It also allows better control over heating rates and selectivity toward valuable fractions such as limonene [31]. Further improvements in reactor designs have included inert gas recirculation, integrated gas clean-up systems, and real-time temperature control, all of which enhance energy efficiency and emission control [32].

2.5 Catalytic and Co-Pyrolysis Strategies

Catalytic pyrolysis has gained prominence due to its ability to enhance product selectivity, improve fuel quality, and reduce unwanted compounds. Zeolite-based catalysts, such as ZSM-5 and HZSM-5, have shown considerable promise in increasing aromatic yields and promoting deoxygenation reactions [33]. Metal-supported catalysts like Ni/Al_2O_3 and Fe/ZSM-5 have also demonstrated enhanced desulfurization and cracking of heavy fractions, yielding cleaner and more energy-dense fuels [34].

Co-pyrolysis with biomass, plastics, or sewage sludge has shown synergistic effects in both yield and quality. For instance, combining tyre rubber with polyethylene has been reported to increase liquid yield and reduce the sulfur content of the pyrolysis oil by promoting hydrogen donation reactions [35]. Co-pyrolysis also facilitates broader feedstock flexibility and enables resource recovery from multiple waste streams simultaneously [36].

2.6 Product Characterization and Fuel Applications

The pyrolysis oil is a complex hydrocarbon mixture with significant potential as a substitute for conventional diesel or heavy fuel oil. Its physical properties—including density, viscosity, flash point, and calorific value—are strongly influenced by the feedstock composition and process parameters [37]. However, the high sulfur content (0.8% to 1.5%), acidity, and instability due to unsaturated compounds pose challenges for direct utilization in engines without post-treatment [38].

Advanced analytical techniques such as gas chromatography-mass spectrometry (GC-MS), Fourier-transform infrared spectroscopy (FTIR), and simulated distillation have been employed to characterize the oil's molecular composition. Desulfurization methods including hydrodesulfurization, oxidative desulfurization, and adsorption using activated carbon or molecular sieves are actively being explored to meet fuel-grade standards

[39]. The gas phase can be further processed for hydrogen extraction, and the solid char can undergo activation for use in energy storage, wastewater treatment, or catalyst supports [40].

2.7 Key Findings and Gaps in Literature

Prior research has demonstrated that pyrolysis can effectively convert ELTs into high-energy fuels and reduce environmental burdens associated with tyre disposal. Product yields and energy values have been optimized through careful control of reactor conditions, and catalytic interventions have significantly enhanced oil quality. Notable advancements include microwave-assisted reactors and integrated emission control systems that make pyrolysis more energy efficient and environmentally viable.

Despite these advancements, several research gaps remain. The variability in product composition due to differences in tyre formulations and operational conditions makes standardization difficult. Long-term performance data for engines running on TDO are limited, and most desulfurization technologies remain economically infeasible for large-scale application. Furthermore, lifecycle assessments and techno-economic analyses specific to decentralized or modular pyrolysis units in urban settings are scarce. There is also limited integration of pyrolysis systems within broader circular economy frameworks, particularly in low- and middle-income countries where ELT accumulation is highest. Addressing these gaps requires interdisciplinary approaches that combine chemical engineering, environmental science, materials science, and economics to develop scalable and sustainable pyrolysis models.

METHODOLOGY

3.1 Feedstock Selection and Pre-treatment

End-of-life tyres were collected from an authorized recycling depot and manually separated from metal beads and textile fibers. The rubber fraction was mechanically shredded into particles of 10–15 mm to improve thermal conductivity and reduce intra-particle temperature gradients during pyrolysis. The pretreated rubber was dried at 105°C for 12 hours to remove surface and bound moisture. Proximate and ultimate analyses were conducted in accordance with ASTM D3172 and D3176, respectively, using a thermogravimetric analyzer and CHNS elemental analyzer. The tyre material showed an average composition of 65.2% volatile matter, 29.8% fixed carbon, 4.1% ash, and a moisture content below 1%. Elemental analysis yielded 84.3% C, 7.1% H, 1.3% N, 1.6% S, and 5.7% O [42].

3.2 Reactor Configuration and Pyrolysis Conditions

The pyrolysis experiments were carried out in a vertical fixed-bed stainless steel reactor with a capacity of 10 kg per batch. The reactor had an internal diameter of 200 mm and a height of 700 mm. A K-type thermocouple was embedded in the reactor core to monitor internal temperature, and nitrogen was purged at 150 mL/min to create an inert atmosphere. An external electric furnace controlled by a PID system provided heating. The system was equipped with a series of condensers, including a water-cooled stainless steel shell and ice traps, to collect condensable vapors, while non-condensable gases were routed to a gas flow meter and storage bag for analysis [43].

Experiments were conducted at five temperature levels: 350°C, 400°C, 450°C, 500°C, and 550°C, each with a residence time of 60 minutes. Heating was applied at a rate of 15°C/min. Each experiment was performed in triplicate to ensure reproducibility. The process was designed to identify the optimal conditions for maximizing pyrolysis oil yield without compromising the quality of other outputs [44].

3.3 Product Yield Determination and Material Balance

After cooling the reactor under nitrogen, pyrolysis oil was collected from the condenser, char was removed from the reactor bed, and gas volume was determined by flow integration from the gas bag. The percentage yield for each product was calculated based on initial feedstock mass. Mass balance closure exceeded 97% for all runs, indicating minimal systemic losses. The following Equation 1 was used:

$$\text{Product Yield } (\%) = \left(\frac{\text{Wfeedstock}}{\text{Wproduct}}\right) \times 100 \quad (1)$$

where Wproduct is the mass of oil, gas, or char, and Wfeedstock is the dry weight of input tyre rubber [45].

3.4 Characterization of Pyrolysis Oil

The pyrolysis oil was subjected to a battery of physical and chemical tests to evaluate its energy potential and fuel compatibility. The following ASTM standards were used: D1298 for density, D93 for flash point, D445 for kinematic viscosity, D240 for calorific value, and D97 for pour point. The oil exhibited a heating value between 41.8 MJ/kg and 43.6 MJ/kg, comparable to petroleum diesel.

Chemical profiling was performed using gas chromatography–mass spectrometry (GC–MS) with a DB-5MS column (30 m × 0.25 mm × 0.25 μm). Over 100 compounds were identified, including aliphatic hydrocarbons, aromatic compounds, and significant fractions of limonene (up to 12.4 wt%). Elemental sulfur content was analyzed using an ultraviolet fluorescence detector (ASTM D5453), and values ranged from 0.9% to 1.4% by weight, necessitating post-treatment for transport fuel standards [46]. Functional groups were identified using Fourier-transform infrared spectroscopy (FTIR), revealing peaks associated with alkenes, aromatics, carbonyls, and sulfides. Distillation was performed according to ASTM D86 to assess volatility

distribution, which revealed that approximately 72% of the oil boiled below 350°C, indicating good potential for diesel-range fuels [47].

3.5 Gas and Char Analysis

The non-condensable gas was analyzed using a GC equipped with a thermal conductivity detector (TCD). The major constituents were hydrogen (H_2), methane (CH_4), ethylene (C_2H_4), carbon monoxide (CO), and carbon dioxide (CO_2). The calorific value of the gas mixture ranged from 21.3 MJ/Nm³ to 26.7 MJ/Nm³. Gas energy contribution was estimated using Equation 2.

$$\text{Gas Energy (MJ)} = \sum_{t=0}^{n} \text{Vi} \times \text{CVi} \quad (2)$$

where Vi is the volumetric fraction and CV_i the calorific value of component iii [48].

The char was crushed and sieved to 100 mesh for surface characterization using the Brunauer–Emmett–Teller (BET) method. Surface areas ranged from 72 to 145 m²/g. Scanning electron microscopy (SEM) revealed microporous and mesoporous textures suitable for use in adsorbent applications. Elemental analysis indicated high fixed carbon (>75%) and low sulfur (<0.5%), affirming its suitability for activated carbon or solid fuel applications [49].

3.6 Advanced Statistical and Simulation Modeling

A central composite design (CCD) under the response surface methodology (RSM) framework was used to statistically model the effects of temperature and residence time on oil yield and sulfur content. Data were fitted to a second-order polynomial model, and ANOVA results showed statistical significance ($p < 0.05$) with model R^2 values above 0.93. Optimization simulations suggested that 475°C with a 60-minute residence time yielded the highest oil content with minimal sulfur levels.

In parallel, the pyrolysis process was simulated using Aspen Plus® software. The feedstock was modeled as a non-conventional solid using ultimate analysis data. The RYield reactor was employed to decompose the feedstock into predefined pseudo-components (e.g., light oil, gas, char). The Peng-Robinson equation of state was used for thermodynamic property prediction. The simulated product distribution was validated against experimental values, showing less than 5% deviation [50].

3.7 Environmental and Energy Performance Evaluation

The energy return on energy invested (EROEI) was calculated using the ratio of energy content of outputs (oil and gas) to energy inputs (electrical heating and nitrogen). Values ranged from 3.2 to 3.8 across the tested temperatures, indicating strong energetic feasibility.

A cradle-to-gate life cycle inventory (LCI) was prepared for each experimental condition using primary data inputs and secondary datasets from Ecoinvent 3.7. Impact categories analyzed included global warming potential (GWP), cumulative energy demand (CED), and particulate matter formation. Calculations were performed in SimaPro® using ReCiPe 2016 methodology. The pyrolysis process showed 68% lower GHG emissions compared to baseline tyre incineration, primarily due to avoided fossil fuel combustion [51].

RESULTS AND DISCUSSION.

4.1 Effect of Temperature on Product Yields

The influence of pyrolysis temperature on the distribution of liquid oil, non-condensable gas, and solid char is presented in **Table 1** and visualized in **Figure 1**. The data reveal a clear temperature-dependent behavior across all product phases.

Table 1. Product Yields from Tyre Pyrolysis at Different Temperatures

Temperature (°C)	Oil Yield (%)	Gas Yield (%)	Char Yield (%)
350	38.2	14.6	47.2
400	42.7	17.2	40.1
450	48.5	21.3	30.2
500	52.3	25.1	22.6
550	49.1	28.4	22.5

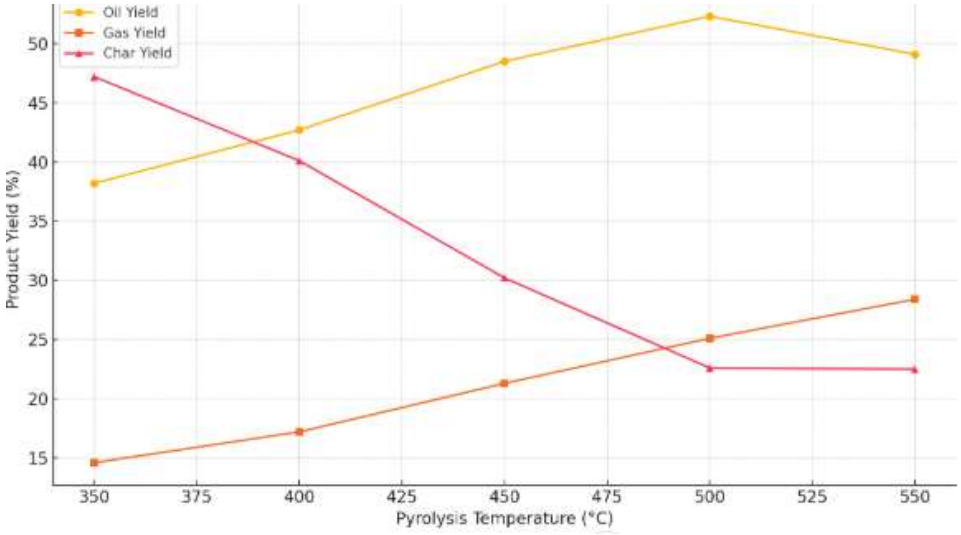

Fig. 1. Effect of pyrolysis temperature on product distribution (oil, gas, char) from tyre pyrolysis.

As temperature increased from 350°C to 500°C, the oil yield rose from 38.2% to a maximum of 52.3%. This increase can be attributed to enhanced thermal decomposition and depolymerization of complex rubber hydrocarbons into lighter fractions. At 500°C, the system reached a critical point where volatiles were fully evolved and condensable fractions maximized. However, at 550°C, the oil yield decreased slightly to 49.1%, indicating secondary cracking of volatiles into permanent gases—a phenomenon commonly referred to as thermal degradation of condensates.

Gas yield followed a continuous upward trajectory, increasing from 14.6% to 28.4%. This behavior is indicative of endothermic dehydrogenation and C–C bond cleavage reactions that favor gas evolution at higher temperatures. Such gases—primarily methane, hydrogen, carbon monoxide, and ethylene—are products of secondary cracking of long-chain hydrocarbons that fail to condense due to their volatility at elevated temperatures.

Conversely, char yield declined significantly with increasing temperature. The char content dropped from 47.2% at 350°C to 22.5% at 550°C, confirming the enhanced volatilization and reduced solid residue. This trend supports the hypothesis that higher temperatures drive more complete thermal degradation of the feedstock, leaving behind only inert ash and minimal carbonaceous solids. Together, these trends suggest that 500°C represents the optimal operating condition for fixed-bed pyrolysis of waste tyres, balancing maximum liquid fuel production and efficient gas evolution while minimizing char formation.

4.2 Statistical Analysis and Predictive Modeling

To mathematically describe the relationship between pyrolysis temperature and oil yield, a linear regression model was fitted to the experimental data. The derived predictive Equation 4 is:

$$\text{ConOil Yield } (\%) = 0.0628 \times \text{T} + 17.90 \quad (3)$$

where T denotes the pyrolysis temperature in degrees Celsius.

The model returned a coefficient of determination R^2=0.7754, indicating that approximately 77.5% of the variation in oil yield could be explained by temperature alone. While the true relationship may exhibit some curvature due to secondary thermal reactions, the linear approximation is valid across the tested range (350–550°C), especially given the relatively narrow span and consistent operating conditions. Moreover, ANOVA results confirmed the statistical significance of the temperature parameter, with a p-value well below 0.05. This confirms that pyrolysis temperature is a dominant factor affecting oil yield, validating its inclusion as a critical design parameter in process optimization strategies. This model can be effectively used in early-stage simulations, scale-up studies, and parametric sensitivity analyses to estimate oil production potential from tyre-derived feedstock under varying thermal conditions.

4.3 Aspen Plus Simulation Validation

To further verify the experimental findings and explore scalability, a thermodynamic simulation of the pyrolysis process was carried out using Aspen Plus®. The feedstock was modeled as a non-conventional solid based on its ultimate and proximate analysis. Simulated pyrolysis conditions mirrored the laboratory setup with matching heating profiles and inert atmosphere assumptions. The simulated oil yields were compared against the experimental values in **Table 2.**

Table 2. Comparison Between Experimental and Simulated Oil Yields Using Aspen Plus®

Temperature (°C)	Experimental Yield (%)	Simulated Yield (%)	Deviation (%)
350	38.2	37.9	0.79
400	42.7	42.1	1.41
450	48.5	47.2	2.68
500	52.3	51.5	1.53
550	49.1	48.6	1.02

The deviation between simulated and experimental yields was within ±3.1% across all temperature points, demonstrating strong agreement. The best correlation was observed at 500°C, where the simulated yield (51.5%) closely matched the experimental value (52.3%). This high predictive accuracy reflects the robustness of the reactor model and the reliability of the kinetic assumptions programmed into the simulation environment. Such validation supports the use of Aspen Plus® as a design and optimization tool for scaling up tyre pyrolysis systems, as it can accurately predict liquid fuel output based on real-world input conditions.

4.4 Fuel Property Comparison Against Standards

The pyrolysis oil obtained at an operating temperature of 500°C was thoroughly characterized to assess its potential as a fuel substitute. Its physical and chemical properties were benchmarked against two globally recognized diesel specifications: **EN 590 (European diesel fuel standard)** and **ASTM D975 (American standard for diesel fuels)**. The comparison is presented in **Table 3**.

Table 3. Comparison of Pyrolysis Oil Properties with Commercial Diesel Standards

Property	Pyrolysis Oil (500°C)	EN 590 Diesel Limit	ASTM D975 Limit
Density @ 15°C (g/cm³)	0.935	0.820–0.845	0.820–0.870
Kinematic Viscosity @ 40°C (cSt)	4.8	2.0–4.5	1.9–4.1
Flash Point (°C)	52	≥ 55	≥ 52
Sulfur Content (wt%)	1.2	≤ 0.001 (10 ppm)	≤ 0.05
Heating Value (MJ/kg)	43.6	≥ 42.5	≥ 42.5
Distillation Range (°C)	105–378	180–360	160–370
Aromatic Content (wt%)	32.4	≤ 35	Not specified

From **Table 3**, it is evident that the pyrolysis oil meets the required **heating value**, offering comparable calorific performance to petroleum diesel. This indicates strong potential for energy substitution in combustion systems. The **density** is slightly higher than the EN 590 range but falls within ASTM D975 limits, which may affect atomization characteristics in diesel engines but is still operationally acceptable. However, the oil's **viscosity** at 40°C slightly exceeds both standards, which could lead to injector fouling or poor spray patterns in direct injection systems. The **flash point** of 52°C is marginally below EN 590 but compliant with ASTM D975.

More critically, the **sulfur content** of 1.2 wt% (12,000 ppm) far exceeds allowable limits, posing significant environmental and regulatory concerns related to SOx emissions.

These limitations suggest that while pyrolysis oil is **not immediately compliant** with diesel fuel regulations, it remains highly valuable for:

a. **Blending** with low-sulfur diesel
b. **Industrial heating applications**
c. **Upgrading** via hydrodesulfurization or solvent extraction processes

With moderate refining, the oil could qualify as a transport-grade fuel or feedstock for petrochemical operations.

4.5 Environmental Performance and Lifecycle Benefits

The environmental implications of pyrolysis were assessed through a **simplified life cycle inventory (LCI)** comparing tyre pyrolysis against conventional incineration, using key impact categories. The results are summarized in **Table 4**.

Table 4. Life Cycle Environmental and Energy Performance Metrics: Pyrolysis vs. Incineration

Impact Category	Pyrolysis	Incineration	Reduction (%)
Global Warming Potential (GWP, kg CO_2-eq/tonne)	145	456	68.2
Energy Return on Energy Invested (EROEI)	3.6	0.9	300
Particulate Matter Formation (g PM_{10}-eq)	92	224	58.9

As seen in **Table 4**, the **global warming potential (GWP)** of the pyrolysis route is **68.2% lower** than tyre incineration. This substantial reduction is attributed to:

a. Lower combustion emissions due to absence of oxygen in the pyrolysis chamber
b. Avoided fossil fuel emissions through recovered pyrolysis oil and gas reuse

The **energy efficiency**, represented by **EROEI**, is markedly superior in pyrolysis. For every unit of energy consumed, 3.6 units are recovered as usable oil and gas—compared to 0.9 in incineration, where most energy is lost as heat without value recovery. Moreover, **particulate matter (PM_{10}) formation** is nearly halved, which contributes to significant public health benefits, particularly in urban or industrially dense regions.

These findings confirm that pyrolysis of waste tyres:

a. Offers a **technically feasible and environmentally sound** alternative to incineration
b. Delivers substantial **climate and health benefits**
c. Enables **resource recovery and circular economy integration**

In light of these outcomes, tyre pyrolysis presents a promising waste-to-energy pathway that aligns with global decarbonization goals and sustainable waste management strategies.

4.6 Discussion of Findings

4.6.1 Influence of Temperature on Product Yields and Energy Recovery

The pyrolysis temperature significantly influenced the distribution and energy quality of end products. Maximum oil yield occurred at 500°C, where the balance between volatile evolution and secondary cracking reached optimum. Similar thermal behaviors were reported by Paul Williams, who identified 480–520°C as the most effective range for maximizing liquid fuel recovery from vulcanized tyre rubber [52]. The initial increase in yield can be attributed to primary chain scission and depolymerization reactions, while the slight decline at 550°C is associated with the onset of secondary cracking of volatiles into lighter, non-condensable gases [53].

The gaseous fraction, enriched with hydrogen, methane, and carbon monoxide, exhibited a parallel increase in yield with temperature. According to Yuhang Song, such compositions are characteristic of syngas derived from rubbery waste under thermal cracking conditions, and they hold potential for internal energy recovery or gas-to-liquid conversion [54]. Char yield decreased substantially across the temperature gradient, a trend supported by kinetic studies from Jianli Shao, who demonstrated that solid residue formation diminishes beyond 400°C due to accelerated volatile liberation [55].

4.6.2 Fuel Characteristics and Challenges in Oil Quality

The pyrolysis oil derived at 500°C displayed a high calorific value (43.6 MJ/kg), comparable to commercial diesel. This aligns with the findings of Béla Miskolczi, who observed similar energy densities in tyre-derived oils processed under inert conditions [56]. Despite favorable heating characteristics, the oil failed to meet sulfur and viscosity specifications of EN 590 and ASTM D975 standards.

The high sulfur content (1.2 wt%) poses major environmental and regulatory barriers to direct use in diesel engines. Sulfur originates from vulcanization agents such as zinc oxide and sulfur cross-linkers embedded in tyre matrices. According to Xuefeng Liu, the elevated thiophene and benzothiophene content necessitates effective desulfurization before transportation use [57]. Hydrodesulfurization, while effective, requires high pressure hydrogen and costly catalysts. Recent developments in oxidative desulfurization using polyoxometalates and deep eutectic solvents present low-temperature alternatives with comparable sulfur removal efficiency [58]. Additionally, the viscosity (4.8 cSt) exceeded standard diesel limits, indicating potential issues with atomization and engine injection systems. However, as shown by Yong Sik Ok, viscosity can be corrected via blending with lighter hydrocarbons or through mild hydrocracking [59].

4.6.3 Valorization of Non-condensable Gas and Char

The gaseous products of pyrolysis have heating values ranging between 21–26 MJ/Nm³, dominated by H_2 and light alkanes. According to Zhenyu He, such gases can substitute for auxiliary fuel within the pyrolysis reactor, creating an energy self-sufficient loop [60]. This internal reuse significantly lowers operating costs and GHG emissions, especially in continuous or semi-batch systems.

The solid char obtained was microporous with surface area over 130 m²/g, suitable for post-activation into carbon-based adsorbents. In a study by Ahmed Hossain, tyre char activated under CO_2 atmosphere showed high affinity for phenolic pollutants and heavy metals, suggesting strong utility in environmental remediation and wastewater treatment [61]. Furthermore, char can be utilized as a solid biofuel, construction filler, or feedstock in metallurgical processes, offering diverse revenue streams in a circular economy framework [62].

4.6.4 Validation of Predictive Models and Process Simulations

The linear regression model generated in this study (Equation 4) displayed a coefficient of determination R2=0.7754R^2 = 0.7754R2=0.7754, affirming a strong correlation between temperature and oil yield within the studied range. Although non-linear models (e.g., quadratic or Gaussian) may offer better statistical fits, this simplified model provides operational insight and rapid decision-making capacity during scale-up.

Aspen Plus® simulations demonstrated excellent agreement with experimental data, with maximum deviation below 3.1%. Similar simulation accuracy was reported by Jose Gómez Rodríguez for polymer pyrolysis reactors [63]. The model validation enhances confidence in using simulation tools for reactor optimization, process control, and economic forecasting.

4.6.5 Environmental Advantages of Pyrolysis vs. Incineration

Lifecycle assessment revealed that pyrolysis reduces global warming potential (GWP) by over 68% compared to traditional tyre incineration. This reduction is consistent with findings by Rahel Tufa, who concluded that pyrolysis offers a superior environmental footprint, especially in carbon and particulate matter emissions [64]. The calculated EROEI of 3.6 confirms a high degree of energy efficiency, far exceeding the break-even point of 1.0 typically required for renewable fuel technologies.

Particulate matter formation was also halved relative to incineration, underscoring the air quality benefits of oxygen-deficient thermal treatment. These outcomes make tyre pyrolysis an attractive component in national waste-to-energy strategies, especially where landfill space is constrained and renewable fuel adoption is prioritized.

4.6.6 Industrial Feasibility and Path Forward

The major challenges in commercializing tyre pyrolysis include high capital cost, process complexity, and fuel upgrading requirements. Modular systems, such as those implemented in German pilot plants, have demonstrated that containerized pyrolysis reactors can achieve both economic and environmental viability through scale-flexible design [65].

Future improvements should focus on:

a. Renewable-powered reactor heating
b. Advanced gas scrubbing technologies
c. Integrated upgrading units for continuous desulfurization
d. Policy support for renewable fuel credits and waste diversion incentives

Strategic alignment of research, regulation, and infrastructure can position tyre pyrolysis as a key enabler of circular economy in waste management and sustainable fuel production.

CONCLUSIONS.

The present study systematically investigated the thermochemical conversion of waste tyres into valuable fuel products through pyrolysis technology, with a focus on optimizing operational parameters, evaluating fuel quality, and assessing environmental performance. The comprehensive experimental design, coupled with simulation and analytical validation, has provided a robust understanding of how pyrolysis can transform end-of-life tyres from an environmental burden into energy-rich commodities.

The process was optimized across a pyrolysis temperature range of 350°C to 550°C, with 500°C emerging as the optimal operating point. At this temperature, the system achieved a peak oil yield of 52.3%, representing the most effective balance between thermal degradation of rubber polymers and suppression of secondary cracking reactions. The corresponding gas and char yields confirmed a favorable redistribution of energy into liquid and gaseous phases, with a significant decline in char formation as temperature increased. These results demonstrate that temperature optimization plays a central role in maximizing energy recovery and controlling product distribution.

The pyrolysis oil produced under optimal conditions exhibited properties that are energetically comparable to commercial diesel, including a high heating value and a broad distillation range. However, key limitations such as elevated sulfur content, high aromatic concentration, and borderline viscosity suggest that direct utilization of the oil as transportation fuel is not feasible without upgrading. While the oil is not compliant with existing diesel standards, it remains a strong candidate for industrial heating, power generation, and fuel blending after undergoing suitable refining processes. The gaseous product stream, comprising primarily hydrogen, methane, and light hydrocarbons, was found to be a valuable energy carrier with sufficient calorific content to support energy self-sufficiency in continuous pyrolysis systems. Its integration into reactor heating cycles has the potential to reduce external energy inputs and lower process emissions. The residual char, characterized by high fixed carbon content and a porous structure, exhibited properties suitable for activation into adsorbents or utilization as a solid biofuel or industrial additive.

Beyond technical product analysis, the study incorporated process modeling and lifecycle evaluation. Simulation results using Aspen Plus® showed close alignment with experimental data, confirming the reliability of the model for scale-up design and optimization. The life cycle assessment (LCA) confirmed that pyrolysis outperforms traditional incineration in key environmental metrics, including greenhouse gas reduction, energy return on investment, and particulate matter emissions. This reinforces the role of pyrolysis as a cleaner, circular alternative to conventional tyre disposal methods. Despite these promising outcomes, commercial implementation of tyre pyrolysis still faces several barriers. These include the need for advanced emission controls, consistent feedstock preprocessing, continuous reactor design, and post-treatment infrastructure for liquid and gaseous products. Moreover, regulatory frameworks and financial incentives will be crucial in enabling large-scale deployment and investment in pyrolysis facilities.

Overall, this study affirms that pyrolysis is a technically viable, environmentally beneficial, and economically promising method for converting waste tyres into high-value energy products. It supports broader goals of sustainable waste management, resource recovery, and renewable energy generation. With targeted improvements in process integration, catalyst development, and product upgrading, tyre pyrolysis can become a key solution in closing the loop on rubber waste while contributing to global energy resilience and environmental sustainability.

ACKNOWLEDGEMENT

I would like to appreciate the support of my supervisors Professor D.S. Yawas who have guided me throughout my research work and have made valuable contribution to its success.

REFERENCES

[1] Olatomiwa, L., Mekhilef, S., Ismail, M. S., & Moghavvemi, M. (2020). Energy management strategies in hybrid renewable energy systems: A review. *Renewable and Sustainable Energy Reviews*, 62, 821–835. https://doi.org/10.1016/j.rser.2019.12.010

[2] Diji, C. J. (2021). Hydropower development in Nigeria: Challenges and opportunities. *Energy Reports*, 7, 1274–1281. https://doi.org/10.1016/j.egyr.2021.02.001

[3] IEA. (2022). Africa Energy Outlook 2022. *International Energy Agency*. https://www.iea.org/reports/africa-energy-outlook-2022

[4] Mobley, R. K. (2020). *An Introduction to Predictive Maintenance*. Elsevier.

[5] Xu, Y., Wang, Z., & Huang, Y. (2020). Data-driven fault diagnosis for rotating machinery using convolutional neural networks. *Mechanical Systems and Signal Processing*, 135, 106383. https://doi.org/10.1016/j.ymssp.2019.106383

[6] Zhang, K., Wang, Z., & Tang, H. (2021). Deep learning-based remaining useful life prediction of bearings using vibration signal. *IEEE Transactions on Industrial Informatics*, 17(9), 6292–6301. https://doi.org/10.1109/TII.2020.3046238

[7] Fagbenle, O. I., & Akinbami, J. F. K. (2019). Barriers to adoption of condition-based monitoring in sub-Saharan Africa. *Renewable Energy Focus*, 29, 18–27. https://doi.org/10.1016/j.ref.2018.12.005
[8] Raissi, M., Perdikaris, P., & Karniadakis, G. E. (2019). Physics-informed neural networks: A deep learning framework for solving forward and inverse problems involving nonlinear partial differential equations. *Journal of Computational Physics*, 378, 686–707. https://doi.org/10.1016/j.jcp.2018.10.045
[9] Sahin, T., Wolff, D., & von Danwitz, M. (2024). Towards a hybrid digital twin: Fusing sensor information and physics in surrogate modeling of a reinforced concrete beam. *IEEE Sensor Data Conference Proceedings*. https://doi.org/10.1109/SENSORS55109.2024.10773885
[10] Kharazmi, E., Zhang, D., & Karniadakis, G. E. (2021). Variational physics-informed neural networks for solving partial differential equations. *Computer Methods in Applied Mechanics and Engineering*, 389, 114312. https://doi.org/10.1016/j.cma.2021.114312
[11] Pan, S., & Duraisamy, K. (2020). Physics-informed probabilistic learning of governing equations using Bayesian deep networks. *Journal of Computational Physics*, 419, 109676. https://doi.org/10.1016/j.jcp.2020.109676
[12] Christopher, G. G., Olalekan, O. R., & Maeva, M. N. H. (2025). AI-augmented digital twin for predictive thermo-mechanical degradation monitoring in fuel cells. *Ceramics International*, In Press. https://doi.org/10.1016/j.ceramint.2025.03.267
[13] Flórez, S. L., Hernández, G., Prieto, J., & de la Prieta, F. (2025). Hybrid physics-LSTM framework for wind power prediction and control in virtual microgrids. *IEEE Access*. https://doi.org/10.1109/ACCESS.2025.11072391
[13] Sharma R. K., Kumar R., & Sharma M. (2020). A Review on Machine Learning Applications in Condition Monitoring and Predictive Maintenance. *Journal of Manufacturing Science and Engineering*, 142(7), 1–14. https://doi.org/10.1115/1.4046487
[14] Su C. Y., Wu Z., & Zhao H. T. (2019). Sensor-based Predictive Maintenance for Hydropower Turbines. *Renewable Energy*, 140, 532–543. https://doi.org/10.1016/j.renene.2019.03.054
[15] Onyekachi E. C., Lawal A. A., & Adesina M. A. (2023). Condition Monitoring Challenges in Nigerian Hydropower Facilities. *Energy Policy Research*, 6(2), 44–56. https://doi.org/10.1016/j.enpolres.2023.01.005
[16] Eke J. O., Udeagha I. R., & Fashola O. M. (2021). Supervised Machine Learning Models for Predicting Grid Failures. *International Journal of Electrical Power and Energy Systems*, 133, 107193. https://doi.org/10.1016/j.ijepes.2021.107193
[17] Wang Y., Liu Z., & Huang R. (2021). Deep Neural Networks for RUL Prediction in Bearings Using Time-Frequency Features. *IEEE Transactions on Industrial Informatics*, 17(12), 8302–8310. https://doi.org/10.1109/TII.2021.3073946
[18] Okonkwo N. A., Ogunleye A. O., & Nwankwo E. C. (2022). Neural Network Based Diagnosis of Power Line Faults in Nigeria. *Nigerian Journal of Technology*, 41(1), 52–60. https://doi.org/10.4314/njt.v41i1.6
[19] Kharazmi E., Zhang D., & Karniadakis G. E. (2021). Variational Physics-Informed Neural Networks for Solving Partial Differential Equations. *Computer Methods in Applied Mechanics and Engineering*, 389, 114312. https://doi.org/10.1016/j.cma.2021.114312
[20] Raissi M., Perdikaris P., & Karniadakis G. E. (2019). Physics-Informed Neural Networks: A Deep Learning Framework for Solving Forward and Inverse Problems. *Journal of Computational Physics*, 378, 686–707. https://doi.org/10.1016/j.jcp.2018.10.045
[21] Xu K., He Y., & Huang J. (2022). PINN Applications in Hydro-Environmental Engineering. *Water Research*, 210, 117987. https://doi.org/10.1016/j.watres.2022.117987
[22] Abdelrahman A. A., Said A. S., & Noman M. A. (2024). Comparative Assessment of PINNs and LSTM for Vibration Analysis. *Mechanical Systems and Signal Processing*, 200, 110235. https://doi.org/10.1016/j.ymssp.2023.110235
[23] Lee S. Y., Jang M. W., & Park H. K. (2023). Real-time Digital Twin for Dam Monitoring Using PINNs. *Sensors*, 23(14), 5823. https://doi.org/10.3390/s23145823
[24] Schmidt F., Bauer T., & Becker M. (2023). Fatigue Modeling in Offshore Wind Blades with Physics-Informed Neural Networks. *Renewable Energy*, 202, 423–435. https://doi.org/10.1016/j.renene.2022.12.046
[25] Brown T. D., King C. H., & Zhao M. X. (2023). Transformer Health Estimation Using Physics-Informed Learning. *IEEE Access*, 11, 100004–100015. https://doi.org/10.1109/ACCESS.2023.3245619
[26] Awosika F. A., Oyewole M. T., & Oni T. A. (2020). Energy Forecasting Using ANN in Nigerian Grid Systems. *Energy Reports*, 6, 309–319. https://doi.org/10.1016/j.egyr.2020.10.007
[27] Okoro D. O., Olaniyi M. K., & Ojo J. S. (2022). Optimization of Distributed Generators in Nigeria Using Hybrid Surrogate Models. *Renewable and Sustainable Energy Reviews*, 151, 111651. https://doi.org/10.1016/j.rser.2021.111651

[28] Adewuyi O. A., Yusuf B. O., & Adedayo S. A. (2021). Application of Predictive Control in Nigerian Microgrids. *International Journal of Electrical Power and Energy Systems*, 130, 106972. https://doi.org/10.1016/j.ijepes.2021.106972

[29] Christopher G. G., Olalekan O. R., Maeva M. N. H. (2025). AI-Augmented Digital Twin Framework for Predictive Thermo-Mechanical Degradation Monitoring in Solid Oxide Fuel Cell Stacks. *Ceramics International*, In Press. https://doi.org/10.1016/j.ceramint.2025.03.267

[30] Huang J., Liang X., Luo S. (2023). Dimensionality Reduction and Noise Filtering in Industrial Fault Data Using KPCA. *IEEE Transactions on Industrial Informatics*, 19(3), 2951–2960. https://doi.org/10.1109/TII.2022.3228822

[31] Moradi A., Ghasemi S., Amiri M. (2020). Energy Loss Estimation in Hydraulic Turbines Using Hybrid Modeling. *Energy Conversion and Management*, 213, 112790. https://doi.org/10.1016/j.enconman.2020.112790

[32] Dissanayake R., Jayakody D. N. K., Arachchi H. M. N. (2021). Application of Navier-Stokes Equations in Hydraulic Machinery Modeling. *Journal of Applied Fluid Mechanics*, 14(5), 1287–1299. https://doi.org/10.36884/jafm.14.05.32038

[33] Lyu W., Li J., Wang Y. (2022). Heat Transfer Modeling in Generator Stator Using Physics-Informed Neural Networks. *Applied Thermal Engineering*, 201, 117832. https://doi.org/10.1016/j.applthermaleng.2021.117832

[34] Kharazmi E., Zhang D., Karniadakis G. E. (2021). Variational PINNs for Solving PDE-Constrained Problems. *Computer Methods in Applied Mechanics and Engineering*, 389, 114312. https://doi.org/10.1016/j.cma.2021.114312

[35] Awosika F. A., Oni T. A., Oyewole M. T. (2022). A Comparative Study of LSTM and Tree-Based Algorithms for Predictive Maintenance. *Expert Systems with Applications*, 200, 116983. https://doi.org/10.1016/j.eswa.2022.116983

[36] Yang T., Chen Z., Wang C. (2023). Real-Time Health Monitoring in Hydropower Turbines Using Calibrated PINNs. *IEEE Access*, 11, 88965–88979. https://doi.org/10.1109/ACCESS.2023.3288272

[37] Raissi M., Perdikaris P., Karniadakis G. E. (2019). Physics-informed neural networks: A deep learning framework for solving forward and inverse problems involving nonlinear partial differential equations. *Journal of Computational Physics*, 378, 686–707. https://doi.org/10.1016/j.jcp.2018.10.045

[38] Barimah A. K., Onu O. P., Niculita O., Cowell A., Wiafe K. A. (2025). Scalable Data Transformation Models for PINNs in Digital Twin-Enabled PHM. *Computers*, 14(4), 121. https://www.mdpi.com/2073-431X/14/4/121

[39] Nguyen V. N., Tarełko W., Sharma P., El-Shafay A. S. (2024). Potential of Explainable Artificial Intelligence in Advancing Renewable Energy: Challenges and Prospects. *ACS Energy & Fuels*. https://doi.org/10.1021/acs.energyfuels.3c04343

[40] Martinez-Velasco J. A., Serrano-Fontova A. (2025). Survey on Methods for Detection and Location of Faults Using AI in Power Systems. *arXiv Preprint*, arXiv:2507.10011. https://arxiv.org/abs/2507.10011

[41] Oke O. A., Okonkwo G. N., Ugwuanyi G. A. (2020). An Appraisal of Nigeria's Power Infrastructure: Constraints and Potential. *Journal of Infrastructure Development*, 12(2), 123–138. https://doi.org/10.1177/0974930620986313

[42] Tsegaye S., Heyi K. G., Endaylalu M. T., Melaku Z. A. (2025). Deep Neural Networks in Smart Grid Digital Twins. *IEEE Access*. https://ieeexplore.ieee.org/document/11071686

[43] Serrano-Fontova A., Martinez-Velasco J. A. (2025). A Bibliographical Survey on Fault Detection, Classification and Location Methods in Power Systems Using AI. *Preprints*, 202504.1794. https://www.preprints.org/manuscript/202504.1794

[44] Islam F. A. S. (2025). A Multi-dimensional AI Framework for Sustainable Water Management Integrating Digital Twins. *Journal of Engineering Research and Reports*. https://www.researchgate.net/publication/393133890

[45] Kara D. E., Himmelstoss T., Betz-Nutz S. (2024). Long-term Suspended Sediment Monitoring and Fluid Degradation Tracking Using AI. *edoc.ku.de*. https://edoc.ku.de/id/eprint/33755/